Understanding the Effects of Concentration on the Solvation Structure of Ca^{2+} in Aqueous Solution. I: The Perspective on Local Structure from EXAFS and XANES

John L. Fulton* and Steve M. Heald

Fundamental Science Division, Pacific Northwest National Laboratory, Richland, Washington 99352

Yaspal S. Badyal and J. M. Simonson

Chemical Sciences Division, Oak Ridge National Laboratory, Oak Ridge, Tennessee 37831-6110

Received: October 16, 2002; In Final Form: March 12, 2003

X-ray absorption fine structure (XAFS) spectroscopy was used to probe the effects of concentration on the first-shell structure of Ca^{2+} in aqueous solution. Measurements were carried out under ambient conditions using a bending magnet beamline (sector 20) at the Advanced Photon Source, Argonne. The Ca K-edge EXAFS spectrum for 6 *m* $CaCl_2$ yielded no evidence for the formation of significant numbers of $Ca^{2+}-Cl^-$ contact ion pairs even at such high concentration, a result confirmed by comparison with the data for a dilute (0.2 *m*) reference solution of the perchlorate. A mean coordination number of 7.2 ± 1.2 water molecules and an average Ca−O distance of 2.437 ± 0.010 Å were determined for 6 *m* $CaCl_2$, and these parameters are also consistent with earlier EXAFS measurements on dilute Ca^{2+} solutions. Comparison of the pre-edge and near-edge (XANES) spectrum against those for various references, including the crystalline hydrates, provided further confirmation of the lack of change in the Ca^{2+} first-shell structure and symmetry. Our measurements help clarify the earlier results of modeling thermodynamic data that imply that some significant structural change occurs at high salt concentration. Taken together, our results suggest the formation of $Ca^{2+}-OH_2-Cl^-$ *solvent-shared* ion pairs, rather than $Ca^{2+}-Cl^-$ contact ion pairs, is most likely responsible for the unusual thermodynamic behavior of this system. The EXAFS spectrum for an even more concentrated (9.2 *m* $CaCl_2$) hexahydrate melt, however, did indicate the presence of some contact ion pairs. The new results agree closely with those of an earlier X-ray diffraction study, and serve to further aid interpretation of the aqueous solutions data. On a technical note, a previously unreported multielectron excitation edge at $k = 10.2$ Å^{-1} was detected in the EXAFS spectra and assigned to the $KL_{II,III}$ transition. Inclusion of this new transition, along with the other known ($KM_{II,III}$ and KM_I) transitions, in the background correction procedure significantly improved the quality of EXAFS fits. Further improvements resulted from the inclusion of Ca−H single scattering paths to treat the protons on the tightly bound water molecules. A Ca−H distance of 2.97 Å was obtained, which is in excellent agreement with the results of neutron scattering measurements (reported in part II). This appears to be the most convincing evidence to date for the detection of proton backscattering in EXAFS measurements of the local structure around ions in aqueous solution.

Introduction

The Ca^{2+} ion is ubiquitous in nature, for example, as an important component of natural groundwaters. The calcium ion is also the most abundant cation in the human body, where it plays a vital role in many biochemical processes including muscle and nerve action. It comes as no surprise then that several structural studies have been made of the hydrated ion using a variety of techniques including X-ray absorption fine structure (EXAFS),[1,2] wide-angle X-ray scattering (WAXS),[3,4] and neutron diffraction isotope substitution (NDIS).[5] Despite this attention, there is wide disagreement regarding such basic parameters of the hydration structure as the mean Ca−O nearest-neighbor distance and average water coordination number. The problem of the Ca^{2+} hydration structure is made difficult by the weak and asymmetric nature of the Ca−O interaction.[6] This difficulty appears to be compounded by differences in experimental technique and interpretation, leading to the wide variation in reported results. A further source of confusion may be the strong concentration dependence of the hydration structure reported in an early NDIS study of 1.0, 2.8, and 4.5 molal (*m*, mol/kg water) calcium(II) chloride aqueous solutions by Hewish et al,[5] although this claim has yet to be verified. The most recent study, by Jalilehvand et al.,[1] employed a combined EXAFS, WAXS, and molecular dynamics (MD) simulation approach to investigate $CaCl_2$ aqueous solutions up to a concentration of 2 mol/dm^{-3}. The findings from the simulation part of this study support a mean Ca−O distance of 2.46 Å and an average water coordination number of 8 at these relatively low concentrations.

Although the focus of earlier studies has largely been on dilute solutions, given the weakly hydrating nature of the Ca^{2+} ion it seems reasonable to expect additional, interesting behaviors at high concentrations up to the saturation solubility of 7.2 *m* at room temperature (25 °C).[7] Using ion interaction (Pitzer) equations, Phutela and Pitzer have demonstrated an anomalous behavior in the osmotic coefficient of aqueous $CaCl_2$ solutions, beginning at around 4.5 *m* concentration, particularly as compared to solutions of another simple salt, $MgCl_2$.[8] The ion interaction approach makes use of the general similarity of

* Corresponding Author. Fax: 509-376-0418. E-mail: john.fulton@pnl.gov.

10.1021/jp0272264 CCC: $25.00 © 2003 American Chemical Society
Published on Web 05/17/2003

nonideal solutions to imperfect gases, an analogy first pointed out by McMillan and Mayer,[9] and involves a virial type of expansion in powers of concentration. Unlike the virial expansion for nonideal gases, however, the terms in the ion interaction model cannot be simply related to intermolecular forces or derived directly from statistical mechanics. Even with these limitations, this empirical approach has proved successful in modeling the properties of many electrolyte solutions up to high concentration. Phutela and Pitzer[8] ascribe the anomalous behavior of concentrated $CaCl_2$ aqueous solutions to some distinct change in hydration structure, perhaps arising from the formation of significant numbers of cation−anion contact ion pairs as Cl^- ions move into the inner shell around Ca^{2+}. The formation of such contact ion pairs has of course been observed in high-temperature aqueous solutions where the reduced dielectric constant of water inevitably leads to increased ion association.[10,11] Although it would seem reasonable to expect a similar effect with increased concentration in room-temperature $CaCl_2$ solutions (because of the dwindling number of water molecules available for completing the hydration shells around each ion), there is currently no supporting evidence. Yamaguchi et al.[3] have conducted WAXS measurements on concentrated $CaCl_2$ solutions and their model fit to room-temperature data for a 6.45 *m* concentration sample suggests the Ca^{2+} hydration structure is little different from that in dilute solution, with no significant level of contact ion-pairing. In light of the ambiguities involved in modeling total scattering data, there is a clear need for further investigation of this problem using methods that provide information specific to the local environment around the Ca^{2+} ion. One such element-specific, but short-range, probe is EXAFS, and our investigation of concentrated $CaCl_2$ aqueous solutions using this technique forms the subject of the present paper.

EXAFS provides detailed information on local structure such as the mean nearest-neighbor distance, symmetry, and coordination number of the first shell around an absorbing atom. In this paper, we report the results of Ca K-edge EXAFS measurements on a concentrated 6 *m* $CaCl_2$ aqueous solution. All measurements were carried out at, or near, ambient conditions on a bending magnet beamline (sector 20) at the Advanced Photon Source (APS), Argonne. The primary goal was to search for evidence of contact ion pair formation in concentrated solutions. The opportunity was also taken to explore the effects of including scattering contributions from nearby hydrogen atoms, a comparatively recent development in EXAFS analysis,[12,13] to see if this resulted in an improved model fit and whether a mean Ca−H distance consistent with NDIS studies could be obtained. To facilitate the primary goal, ancillary measurements were made using crystalline reference compounds including the dihydrate and hexahydrate of $CaCl_2$. To establish a reference for which there could be no possibility of Cl^- appearing in the inner shell around Ca^{2+}, a dilute (0.2 *m*) aqueous solution of the perchlorate, $Ca(ClO_4)_2$, was also measured. In addition, the fused hexahydrate salt, $CaCl_2{\cdot}6(H_2O)$, was measured at a temperature just slightly above its melting point (28 °C) to serve as a higher-concentration (9.25 *m*) reference. Finally, a mixed solution of 0.7 *m* $CaCl_2$ and 5.0 *m* $MgCl_2$ was studied in order to examine the effects on the Ca^{2+} hydration structure of competition for waters of hydration from large numbers of more strongly hydrated magnesium ions. The X-ray absorption pre-edge and near-edge structure (XANES) also provides information on the first coordination shell, and our findings are discussed below in conjunction with the interpretation of the EXAFS data.

In a companion paper[14] (henceforth referred to as II), we describe the results of a complementary study using neutron diffraction and calcium isotope substitution. The results of that study, when taken together with the information on local order from the present EXAFS work, provide a more complete and longer-range picture of Ca^{2+} hydration in concentrated solution. The common purpose of our investigations was to gain new insights into the underlying microscopic basis of the apparent anomaly in thermodynamic behavior at high salt concentration.

Experimental Methods and Theory

Sample Preparation. Part of the analysis involved studies of well-characterized reference compounds including $CaCl_2$, $CaCl_2{\cdot}2(H_2O)$, and $CaCl_2{\cdot}6(H_2O)$. The calcium chloride salt was obtained in the ultra-dry form from Alfa Aesar (99.9% purity), and the dihydrate (99.5% purity) from EM Science. The hexahydrate was grown at room temperature by slow crystallization from a concentrated (6.8 *m*) $CaCl_2$ solution kept under partial vacuum in a desiccator. Because both the pure salt and the dihydrate are deliquescent, handling of these compounds took place in a dry glovebox. To limit changes in water content during measurement, the solids were ground up and mixed with a high-purity, hydrocarbon grease (Apiezon Type H). This powder/grease matrix provides an effective diffusional barrier against water, at least for the short time required to obtain several XAFS spectra. The melting point for the hexahydrate is 28 °C, and grinding of this material to produce a powder required a cooled mortar and pestle to eliminate pressure- or friction-induced melting. The 6 *m* $CaCl_2$ aqueous solution was made up by dilution from a concentrated stock solution initially prepared from the dihydrate (EM Science) using distilled, deionized water. The concentration of this stock solution was checked both by comparison of the measured density at 25 °C and 1 bar to previous measurements in the literature, and by desiccation. The $Ca(ClO_4)_2$ solution was prepared by weighing using the tetrahydrate (Sigma-Aldrich, 99% purity) and Nanopure water. To make up the $CaCl_2-MgCl_2$ solution, a concentrated solution of $MgCl_2$ was prepared from the hexahydrate, $MgCl_2{\cdot}6H_2O$ (Mallinckrodt, ACS grade). The concentration of this solution was checked by atomic absorption spectroscopy before it was combined with the $CaCl_2$ stock solution. Throughout this paper, concentrations are expressed in molality, *m* (mol/kg water).

XAFS Methods. For concentrated samples containing low-*Z* atoms such as Ca, the fluorescence XAFS spectra are prone to self-absorption effects that cause *k*-dependent reductions in the XAFS amplitudes. Corrections can be applied to account for this effect.[15,16] Both fluorescence and transmission spectra were acquired for all samples. In general, the transmission measurements required no corrections to the XANES or XAFS spectra since the absorption edge height, $\Delta\mu x$, was below 1.5 in all cases as required to eliminate leakage effects.[16]

For the transmission measurements, a special cell was constructed for the liquid samples. A "U"-shaped Kapton spacer having a thickness of 50 or 275 μm was used to define the transmission path lengths. This spacer was about 6 mm long by 4 mm high with a small slot cut in from one end to allow introduction of the sample. The liquid sample was contained within this spacer by two, 13 μm thick Kapton transmission windows. After the liquid sample was injected into the cell with a micro-liter syringe, the thin transmission windows were tensioned using a small mechanism similar in design to a drumhead tensioner. This arrangement satisfied the twin goals of (a) providing highly parallel transmission windows and (b) squeez-

TABLE 1: Results of Ca XAFS Analysis of the Ca^{2+} First Shell Structure Under Ambient Conditions. The concentrations are expressed in molality

system					structure						
ID	$[Ca^{2+}]$	$[Cl^-]$	$[ClO_4^-]$	$[Mg^{2+}]$	scatterer	N	R, Å	$\sigma^2 \times 10^3$, Å^2	$C_3 \times 10^3$, Å^3	φ	$\mathcal{R}$ [a]	k-weight
A	0.2	--	0.4	--	oxygen	6.8(0.5)	2.436(009)	9.9(1.8)	3.7(3.9)		0.04	2
B[b]	0.2	--	0.4	--	oxygen	8.2(0.6)	2.429(008)	11.4(1.2)	1.0(2.4)	51°(6)	0.03	3
					hydrogen	16.4[c]	2.937(040)	11.9(6.4)	--			
C	6.0	12.0	--	--	oxygen	7.2(0.6)	2.440(009)	10.5(1.8)	3.8(4.0)		0.04	2
D[b]	6.0	12.0	--	--	oxygen	8.4(0.4)	2.437(005)	11.9(0.8)	3.0(1.6)	47°(3)	0.01	3
					hydrogen	16.8[c]	2.965(020)	9.6(2.9)	--			
E[d]	0.7	11.4	--	5.0	oxygen	6.6(0.4)	2.441(010)	8.1(1.9)	3.0[e]		0.05	2
					chlorine	0.4(0.6)	2.727(046)	4.4(12.0)	--			
F[d]	molten $CaCl_2 \cdot 6(H_2O)$ T = 32 °C				oxygen	5.5(0.6)	2.440(010)	10.2(2.1)	3.0[e]		0.05	2
					chlorine	1.2(0.5)	2.746(016)	7.0(4.5)	--			

[a] Goodness of fit defined by a scaled sum of squares as described in FEFFIT.[23] [b] Re-analysis of $CaCl_2$ solution data including single scattering paths for Ca-H and with the spectrum corrected for three multi-excitation edges. [c] Fixed in the fitting at twice the oxygen coordination number. [d] This measurement was acquired in fluorescence mode where appropriate corrections to the amplitude and the Debye-Waller factor have been applied. Other measurements were acquired in transmission mode. [e] Fixed in fitting.

ing the solution so that the path length was defined by the spacer thickness. For the fluorescence measurements of the liquid samples, a window film of 6 μm thick polypropylene was used to cover the opening in the nylon cell. This fluorescence cell was then used in a standard detector arrangement.[16]

Calcium K-edge (4038.5 eV) XAFS spectra were collected on a bending magnet beamline (Sector 20) run by the Pacific Northwest Consortium—Collaborative Access Team (PNC-CAT) at the APS, Argonne. A single 20-minute scan was sufficient to obtain high-quality transmission spectra at this facility, whereas about 10 scans were averaged for the fluorescence spectra. Harmonic rejection is especially important at low energies so a 40 cm long, Rh-coated X-ray mirror was inserted just in front of the I_0 detector and set to 0.57°. When combined with crystal detuning, such a mirror provides harmonic rejection of better than 10^5. Energy calibration was accomplished using the first inflection point of a V foil spectrum (5463.76 eV). An absolute encoder ensured the linearity of the monochromator calibration from this energy down to that of the Ca K-edge. With this method, the first inflection in the spectra (transmission) for the dilute aqueous Ca^{2+} solutions was located at 4042.52 eV.

We used standard methods for the analysis of EXAFS data[17−19] using portions of the UWXAFS program.[20] The EXAFS relationship is given by

$$\chi(k) = \sum_i \frac{F_i(k) S_0^2 N_i}{kR_i^2} e^{-2k^2\sigma_i^2} e^{-2R_i/\lambda(k)} \sin\left(2kR_i + \delta_i(k) - \frac{4}{3}k^3 C_{3,i}\right) \quad (1)$$

The EXAFS oscillations, $\chi(k)$, were extracted from the experimentally measured absorption coefficient using an automated background subtraction method (AUTOBK) developed by Newville et al.[21] The wavenumber of the ejected photoelectron is given by $k = \sqrt{2m_e(E - E_0)/\hbar^2}$ with E_0 being the absorption edge energy. In eq 1, $F_i(k)$, $\delta_i(k)$, and $\lambda(k)$ are the amplitude, phase, and mean-free-path factors, respectively, that are derived from theoretical standards calculated by FEFF8.[22] The S_0^2 term in the above equation is the core-hole or amplitude-reduction factor and is usually treated empirically. The sum in eq 1 is over all possible single scattering paths and for all the significant multiple scattering paths that are calculated to describe the effective scattering amplitudes and phases. The fitted parameters include N_i, the coordination number of the shell for each type of neighboring atom, R_i, the shell distance, σ_i^2, the Debye−Waller factor which represents the mean-square variation in R_i due to both static and thermal disorder, and finally $C_{3,i}$, the anharmonicity of the pair-distribution. The fitting of the FEFF8 theoretical standards to the experimental data was accomplished using an analysis program (FEFFIT)[20,23] that employs a nonlinear, least squares technique. In addition to the structural parameters, a single nonstructural parameter, ΔE_0, is varied to correct for the simple estimate of E_0 made by FEFF8. For all systems, ΔE_0 was fixed at a best-fit value of 3.8 eV above the 4042.5 eV inflection point described earlier. To estimate the core-hole factor, we used the coordination numbers and distances from crystallographic data[24−26] for the three solid reference compounds as input to the FEFFIT program. The S_0^2 values were then found to be 0.75, 0.65, and 0.68 for $CaCl_2$, $CaCl_2 \cdot 2(H_2O)$ and $CaCl_2 \cdot 6(H_2O)$, respectively. According to eq 1, we see that this much variation in S_0^2 results in an approximate 20% uncertainty in the reported coordination number. For the solution samples, we used a core-hole factor of $S_0^2 = 0.69$, i.e., the average from the three different solid standards. Note that for the solid standards, S_0^2 was determined without correcting the multielectron edges. Therefore, to provide the most accurate estimate of first-shell coordination numbers, the same analysis procedure for this parameter was adopted for the liquid samples. Finally, the solid spectra were not fit with Ca−H scattering paths, as was done for some of the solution spectra because the solid spectra in the low-k region have many interfering contributions from single scattering of the second and higher atomic shells and from multiple scattering.

The values calculated by FEFF8 for the muffin-tin radii of 1.7, 1.0, and 0.8 Å for Ca, O, and H, respectively, were used without modification. An improvement in this latest version of the FEFF code has resulted in more realistic estimates of the muffin-tin radii for the hydrogen and oxygen of the water molecule. The refinement of the water model for the Fermi energy and partial wave phase shifts described by Wilson et al.[12,27] provides a significant improvement in the derived parameters. The contributions from second-shell waters have been ignored because many studies have confirmed that there are no significant effects on the EXAFS spectra due to the longer distances (see terms in eq 1) and much greater disorder associated with this shell.[2,28,29]

The Ca $\chi(k)$ data were weighted by k^2, and windowed between $2.0 < k < 13.0$ Å^{-1} using a Hanning window with $dk = 1.0$ Å^{-1}. The fits were to both the real and imaginary parts of $\tilde{\chi}(R)$ in the region of $1.5 < R < 5.0$ Å. The uncertainties reported in Table 1 correspond to an increase in the misfit (defined by a

scaled sum of squares, χ_{FEFFIT}^2) between the data and the best-fit model by an amount of $1/\nu$, where ν is the degrees of freedom in the fit.[20]

For an aqueous system in which there is a high degree of disorder, the XAFS oscillations are relatively weak and the multielectron excitations[13,30−33] thus represent a larger proportion of the total variation in absorption intensity. For Ca, there are several multielectron excitations and these features must be efficiently removed from the experimental spectra in order to obtain accurate measures of the Debye−Waller factor and anharmonicity of the real-space distribution. One approach is to fit representative functions (e.g., arctan) with 2 or 3 adjustable parameters at each edge to approximate the shape of the multielectron edges. There can be difficulties with this approach since it introduces additional, adjustable parameters into the overall least-squares fit; a problem made worse by the fact that multiple, low-k edges may be convoluted with EXAFS information. Here we apply a variation of this procedure that significantly reduces the number of fit parameters. First, we note that there are strong similarities in the multielectron background functions of nearby atoms (consider, for example, the series Br, Kr, Rb, and Sr[34]) and we employ this observation in using Ar spectra to approximate the Ca^{2+} multielectron features. To achieve this, the multielectron background features of Ar[35] were fit with an arctan + Gaussian ($KM_{II,III}$) and a slope change[31] function (KM_I). The multielectron edge energies from this fit were then rescaled to Ca energies using the $Z + 1$ model for the onset of the multielectron edges. The $Z + 1$ rule, which states that the energy required to eject the second electron after creation of a core-hole vacancy is equal to the binding energy of that electron for the next higher element,[31] accurately predicts such shifts in edge position. A new edge arising from the $KL_{II,III}$ transition, which has not been previously reported for Ca and is not included in the more recent Ar spectra, was clearly identified in the two solid compounds, $CaCl_2$ and $CaCl_2 \cdot 2(H_2O)$. Using the known crystallographic information, the EXAFS contributions in this spectral region were removed yielding the $KL_{II,III}$ function for each solid. The averaged $KL_{II,III}$ edge from these standards was then fit using arctan + slope functions in addition to a "white line" feature at the KM_I edge that was fit with a Gaussian function. Finally, these three multielectron features were combined into a new background function that was scaled to the Ca edge height and then removed from the respective Ca spectra (See Supporting Information, Figure 1S). This method avoids the introduction of *any* additional adjustable parameters and greatly improves the quality of the fits to the EXAFS theoretical standards.

Results and Discussion

EXAFS Evaluation of the Reference Compounds. The EXAFS spectra of the solid reference compounds were used primarily to generate an accurate estimate of S_0^2 that could then be used to determine the water coordination numbers for the aqueous Ca^{2+} systems. Note that all of the other structural parameters, including R_i, σ_i^2, and $C_{3,i}$, were derived from the theoretical standard, FEFF8, and not from the solid standards. Figure 1 shows the k^2-weighted $\chi(k)$ data for the three reference compounds, $CaCl_2$, $CaCl_2 \cdot 2(H_2O)$, and $CaCl_2 \cdot 6(H_2O)$. For comparison, the spectrum of a 0.2 *m* $Ca(ClO_4)_2$ solution is also shown. The dotted lines for the solids in Figure 1 are the fit results for the 6 primary single-scattering paths of the atoms that lie within 5 Å of the Ca, the coordination numbers and distances having been derived from crystallographic information. The crystal structure of $CaCl_2$ is orthorhombic and has six Cl

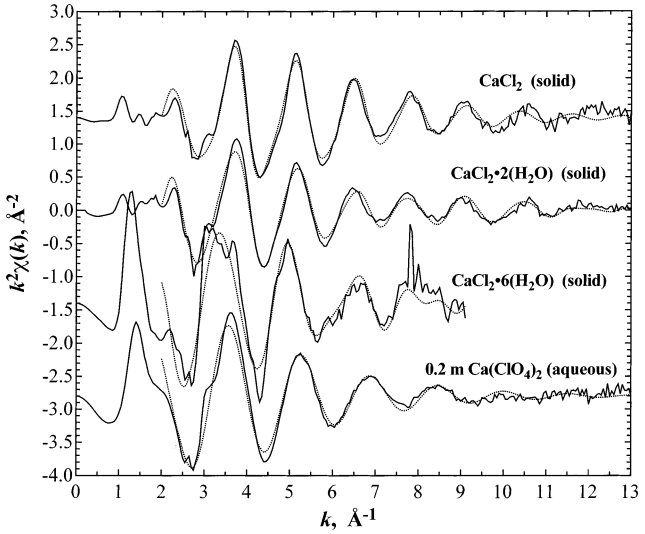

Figure 1. Ca EXAFS k^2-weighted $\chi(k)$ for three solid reference compounds and an aqueous 0.2 *m* $Ca(ClO_4)_2$ solution. The solid lines are the experimental data and the dotted lines represent the fits to the known crystallographic structures. All spectra were acquired in transmission mode and are uncorrected for multielectron edges.

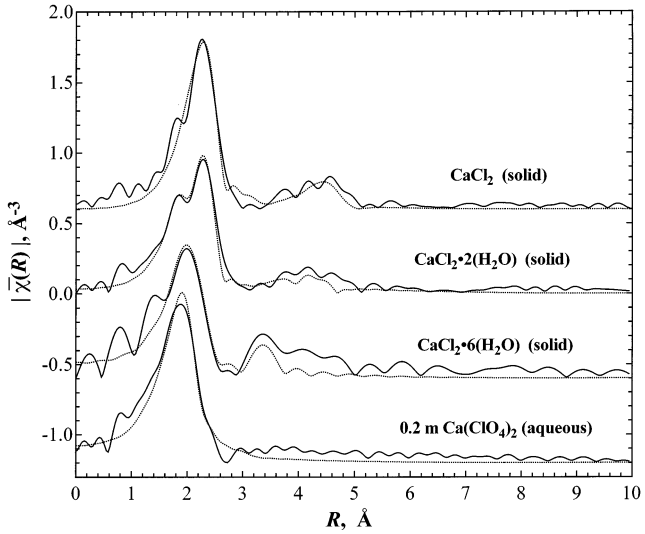

Figure 2. The $|\tilde{\chi}(R)|$ plots corresponding to the spectra shown in Figure 1. The solid lines show the experimental data, and the dashed lines show the fits using FEFF calculations and the crystallographic information. The distances have not been corrected for phase shifts. The unphysical peaks at 0.8 Å are artifacts of the multielectron excitations.

atoms surrounding Ca, four of them lying in an equatorial plane at 2.76 Å, and the remaining two in axial sites at 2.70 Å.[24] In the case of $CaCl_2 \cdot 2(H_2O)$, there are still four Cl atoms in the equatorial plane, at 2.74 Å, but now the two axial sites are occupied by the oxygen atoms of water molecules at a distance of 2.32 Å.[25] The crystal structure of $CaCl_2 \cdot 6(H_2O)$ has Ca surrounded only by water molecules, with no Cl present in the first coordination shell.[26] The 9-fold coordination structure is best described in terms of a right triangular prism with Ca at the center, 6 oxygen atoms residing at the vertices at a distance of 2.59 Å, and a further three oxygen atoms projecting out from the vertical faces at the shorter distance of 2.45 Å. For these compounds, the contributions from Cl and O nearest-neighbor atoms around Ca are qualitatively resolved in the $\tilde{\chi}(R)$ results presented in Figure 2. The $\tilde{\chi}(R)$ functions are generated by Fourier transformation of $\chi(k)$ data and represent the partial pair

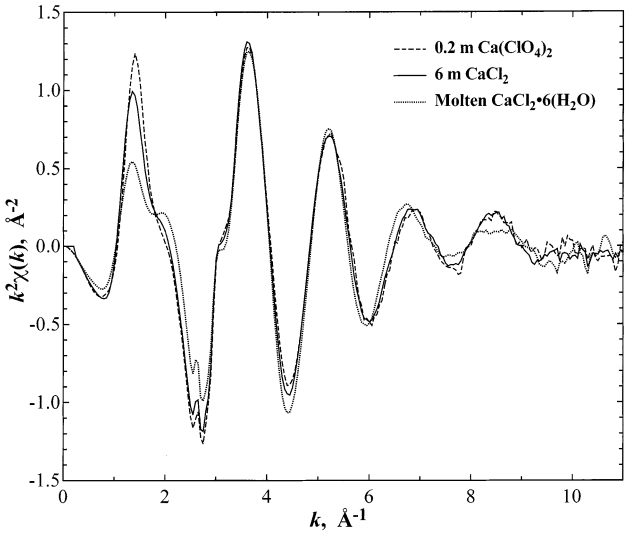

Figure 3. Ca EXAFS k^2-weighted $\chi(k)$ plots for 0.2 *m* $Ca(ClO_4)_2$ and 6.0 *m* $CaCl_2$ aqueous solutions acquired in transmission mode at 25 °C. The plot also included the fluorescence spectrum of molten $CaCl_2 \cdot 6(H_2O)$ (9.25 *m*) at 32 °C. All spectra are uncorrected for multielectron edges. The EXAFS region (but not the XANES region) of the fluorescence spectrum for the molten $CaCl_2 \cdot 6(H_2O)$ has been corrected for self-absorption effects.

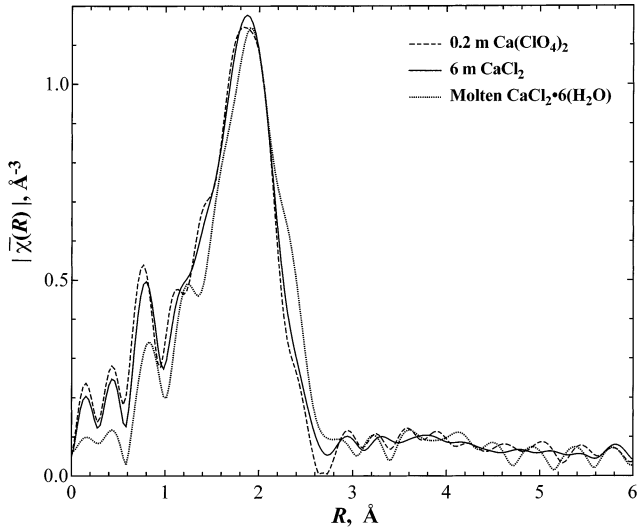

Figure 4. The $|\tilde{\chi}(R)|$ plots derived from the spectra shown in Figure 3 for 0.2 *m* $Ca(ClO_4)_2$ and 6.0 *m* $CaCl_2$ solutions, and for the molten $CaCl_2 \cdot 6(H_2O)$. The $|\tilde{\chi}(R)|$ plot is uncorrected for phase shifts, whereas the corrected distances are reported in Table 1.

distribution functions convoluted with the photoelectron scattering functions shown in eq 1.

The 0.2 *m* $Ca(ClO_4)_2$ solution is now worth discussing in some detail as it will serve as an important reference system for the concentrated $CaCl_2$ solution. The perchlorate ion, ClO_4^-, has a negligible tendency to coordinate with Ca^{2+}, particularly at low concentration and under ambient conditions, hence it is reasonable to assume the calcium ion is fully hydrated in this solution. Even if there were to be some degree of ion association, the nature of the perchlorate anion means that Cl cannot approach close enough to appear as a first neighbor of Ca. Comparing the $\tilde{\chi}(R)$ result for this solution and for the other standard materials (see Figure 2), the following qualitative observations can be made. The Cl peak, clearly discernible at 2.3 Å for the $CaCl_2$ and $CaCl_2 \cdot (H_2O)$ compounds, is absent in the aqueous 0.2 *m* $Ca(ClO_4)_2$ data (note, the distances here are uncorrected for phase shifts). In the case of the perchlorate solution, the water oxygen peak at 1.85 Å is also narrower and at a shorter distance than for the $CaCl_2 \cdot 6(H_2O)$ salt where the first-shell water resides at two different distances, thus giving rise to a longer average distance than for the aqueous system.

EXAFS Analysis of Aqueous Ca^{2+} Solutions. *A Preliminary Comparison of the EXAFS Spectra*. The uncorrected, k^2-weighted $\chi(k)$ data (without multielectron edge background corrections) for the concentrated 6 *m* $CaCl_2$ solution is compared to that of the dilute 0.2 *m* $Ca(ClO_4)_2$ reference in Figure 3. It can be clearly seen that these two spectra, which vary by a factor of 30 in concentration, are virtually identical in the EXAFS region above $k = 2$ Å^{-1}. There is an excellent match in the amplitudes and phases of the oscillations up to $k = 12$ Å^{-1}. This direct comparison provides strong evidence that the first-shell water structure around Ca^{2+} in the concentrated solution is little different from that in the dilute reference solution. A similar agreement is demonstrated in the $\tilde{\chi}(R)$ plot for these two solutions as shown in Figure 4. These preliminary findings are consistent with those of Yamaguchi et al.[3] for a slightly more concentrated 6.45 *m* $CaCl_2$ aqueous solution where a model fit to WAXS data also suggests minimal, contact ion-pairing. As explained in the Introduction, modeling of thermodynamic data by Phutela and Pitzer[8] indicates some type of structural transition in concentrated $CaCl_2$ aqueous solutions beginning around 4.5 *m*. Given the empirical nature of the ion-interaction approach used by these workers, low levels of contact ion-pairing—below the detection limits of either EXAFS or WAXS measurements—may still explain the thermodynamic anomaly. However, even from this preliminary comparison of the EXAFS spectra, it is already possible to discount the original suggestion by Phutela and Pitzer[8] of an abrupt structural change in these solutions involving the formation of *substantial numbers* of contact ion pairs. We now proceed to a more formal and detailed analysis of the data, beginning with a discussion of the multielectron excitations.

Multielectron Excitations. Figure 5 shows k^2-weighted $\chi(k)$ spectra for the 6 *m* $CaCl_2$ aqueous solution obtained using two different background and fitting methods. The solid lines in Figure 5 are the experimental data and the dashed lines are the EXAFS fits with parameters as reported in Table 1. This comparison illustrates the importance of properly correcting for multielectron excitations. For the lower spectrum in Figure 5, only the cubic-spline background function has been removed. In this spectrum, there are three clearly-defined features that are assigned to the $KM_{II,III}$, KM_I, and $KL_{II,III}$ transitions at 2.7, 3.7, and 10.3 Å^{-1}, respectively. As already noted, the $KL_{II,III}$ feature, which is also evident in the spectra of the solid $CaCl_2$ and $CaCl_2 \cdot (H_2O)$ standards, has not previously been reported for Ca XAFS. For the upper spectrum in Figure 5, the multielectron edges have been removed using the procedure described earlier in the Experimental Section (also see Supporting Information, Figure 1S). Of the resulting improvements, the most notable is in the region from $7 < k < 12.5$ Å^{-1} where the oscillations due to the first-shell water are now clearly visible out to high *k*. Because of these improvements, the most accurate values of σ^2 and C_3 are obtained from this spectrum (item D in Table 1).

Figure 6 shows the real-space $\tilde{\chi}(R)$ data corresponding to the $\chi(k)$ spectra in Figure 5. After removal of the multielectron excitations, there are significant improvements in $\tilde{\chi}(R)$. The unphysical peaks at distances below about 1.2 Å are mostly eliminated and the broad feature at 4 Å due to the low-*k*, $KM_{II,III}$ and KM_I edges is significantly reduced. There are also small

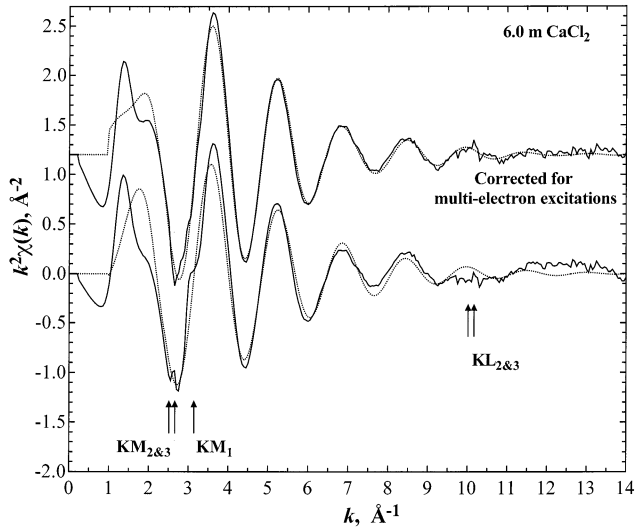

Figure 5. Ca EXAFS k^2-weighted $\chi(k)$ plots for the 6.0 *m* $CaCl_2$ solution. The solid lines represent the experimental data, and the dotted lines are the theoretical fits using the parameters reported in Table 1 ("C" and "D"). The lower spectrum contains the multielectron edges as indicated. In the upper spectrum these features have been removed using the procedure described in the text. The fit to the lower spectrum uses a single Ca−O scattering path and a *k*-weighting of 2. For the upper spectrum, both Ca−O and Ca−H paths are included and the *k*-weighting is increased to 3 to better capture the high-*k* details that contain the significant information on σ^2 and C_3.

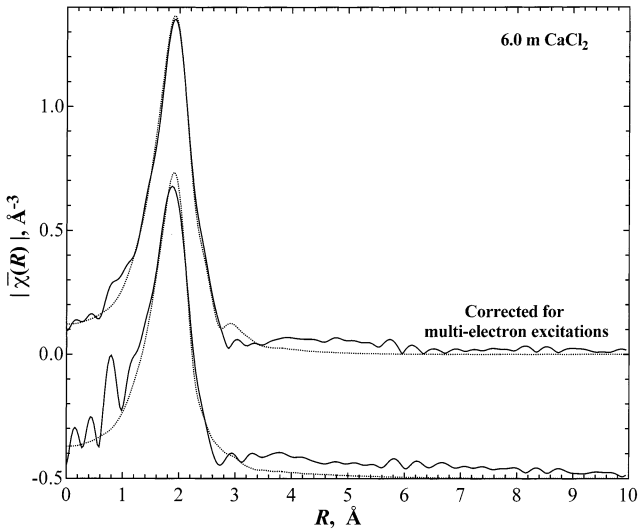

Figure 6. The $|\tilde{\chi}(R)|$ plots derived from the spectra shown in Figure 3 for the 6.0 *m* $CaCl_2$ solution. The experimental data are shown as solid lines and the dashed lines are the fits using the FEFF calculations. The $|\tilde{\chi}(R)|$ plot is uncorrected for phase shifts whereas the corrected distances are reported in Table 1.

changes in the shape of the high-*r* shoulder of the main peak between 2.2 and 2.6 Å.

EXAFS Structural Parameters. Structural parameters derived from fits of the theoretical standards to the experimental data are presented in Table 1. The best estimates of R_{Ca-O}, σ_{Ca-O},[2] and C_3 come from the analyses in "B" and "D" where the multielectron excitations have been removed prior to the EXAFS analysis and the *k*-weighting employed in the fit was increased to 3 to capture the information in the weak oscillations at high *k*. The data reduction methods used in "B" and "D" are also improved by the inclusion of Ca−H scattering paths. The best values for R_{Ca-O} and σ_{Ca-O}^2 are then 2.44 Å and 0.012 Å^2, respectively. These are not significantly different from the corresponding values of 2.46 Å and 0.011 Å^2 reported by Jalilehvand et al.[1] Our value for C_3 of 0.0003 Å^3 is about 3 times smaller than that reported in ref 1. The primary manifestation of C_3 in $\chi(k)$ are small phase shifts in the oscillations above $k = 9$ Å^{-1}.[36] Consequently the best estimate of C_3 would be obtained by utilizing higher *k* data where the region of the interfering $KL_{II,III}$ edge at $k = 10$ Å^{-1} has been removed in the background function. However, C_3 is coupled with E_0 so there are significant uncertainties in this value that are dependent upon the choice of E_0. (See Supporting Information, Table 1S.) Consistent with the preliminary comparison of the $\chi(k)$ spectra in Figure 3, the full EXAFS analysis indicates no appreciable cation−anion pairing. However, in the case of 6 *m* $CaCl_2$, the EXAFS detection limit is about 0.15 Cl atoms around Ca (as evaluated from FEFF analysis of various model systems), thus a limited amount of ion association remains possible in such a concentrated solution.

The best estimate of coordination number comes from analyses "A" and "C" where only the Ca−O scattering paths for the nearest-neighbor water molecules were used to fit the data. In both cases, the treatments of the background function and the fitting methods were identical to those used on the solid reference compounds to estimate S_0^2. The resulting best estimate of the first-shell water coordination number is about 7.0. The uncertainty in this estimate is about 20%, which simply reflects the variation in the values of S_0^2 derived from the solid standards. The estimate of approximately 7 nearest-neighbor waters is in broad agreement with other studies of this system.[3,5]

In accord with previous findings, linear multiple scattering paths for first-shell O neighbors of Ca are not significant. There is also no evidence of contributions from triangular O−Ca−O paths, although the double-return, multiple scattering path for Ca−O does appear to make a slight contribution. This is in marked contrast to the findings for some other metal ions in aqueous solution, particularly the transition elements, where rigid, octahedral symmetries lead to strong multiple scattering contributions.[37−39] Such differences suggest the Ca^{2+} hydration structure is rather disordered, lacking any imposed symmetry either from bonding or packing constraints. Our findings are perhaps not completely surprising given the simple, noble-gas electronic configuration of the Ca^{2+} ion.

Ca−H Scattering. Recent EXAFS studies have indicated there is a small, but measurable, scattering contribution from nearby hydrogen atoms.[12,13] The Ca−H contribution to the overall $\chi(k)$ of aqueous Ca^{2+} occurs at low *k* in the region from $1 < k < 5$ Å^{-1} and the amplitude of the oscillations, resulting from the approximately 14 protons of the hydrating waters, is less than 5% of that from the oxygens (from an evaluation of the $F_i(k)$ values in eq 1 using FEFF8). Although the amplitude is low, we detect a significant signal from the Ca−H scattering paths that is only weakly coupled to the oscillations from the Ca−O paths. We have thus applied this additional analysis to interpretation of the Ca EXAFS spectra in evaluations "B" and "D" in Table 1. The resulting Ca−H distance of 2.97 Å is close to the distance of 3.02 Å reported in an earlier neutron scattering study[5] and is in even better agreement with the more recent results described in paper (II). Our estimate for the Ca−H distance is substantially shorter than the maximum value of approximately 3.12 Å expected from assuming a rigid water molecule in a symmetric, dipole orientation around the Ca^{2+} ion (See Figure 7). Such a reduction in the *mean* ion−hydrogen distance has been observed in a number of neutron scattering studies and is most likely due to the thermally induced "wagging" motions of the hydrogen "legs" of water molecules

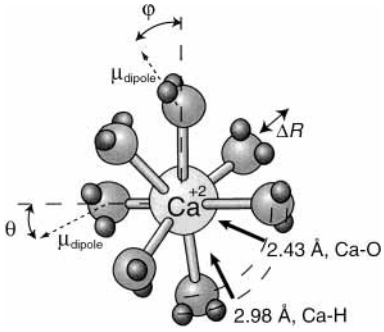

Figure 7. Schematic of the water hydration structure about Ca^{2+} showing those motions of water that lead to dynamic disorder of the Ca−H and Ca−O distances. The interconnecting rods between the water molecules and the Ca^{2+} are included to improve the three-dimensional representation. The quantity ΔR represents the vibrational motion in a radial direction that affects both the Ca−O and Ca−H distances. The angle φ represents the wagging motion of the water protons moving back and forth through a Ca−O−H_2 plane. This mode affects both the mean Ca−H distance and the variance of this distance. The angle θ represents the rocking motion of the water protons in a Ca−O−H_2 plane. This mode primarily affects the variance of the Ca−H distance. μ_{dipole} is the water dipole moment.

surrounding the solute ion.[40,41] Alternatively, there may be a specific ion−water interaction that tends to tilt the water on the ion surface. In a recent ab initio molecular dynamics study of the hydration structure about Mg^{2+}, Lightstone et al.[42] showed that a tilted orientation could be favored by a direct interaction of the oxygen lone-pair electron orbitals with the cation.

The EXAFS measurement of the Ca−H distance in the present study of the Ca^{2+} system provides the first independent verification of the reduced ion−H distance in aqueous solution typically found using the neutron diffraction isotope substitution method. As a further test, the Ca−H structure was also evaluated from the 6 *m* $CaCl_2$ EXAFS spectrum without corrections applied for multielectron excitations in the background function. This analysis yielded a somewhat shorter Ca−H distance of 2.91 Å, thus illustrating that the low-energy multielectron edges are slightly coupled with this parameter and must be properly removed to recover accurate Ca−H distances.

In their EXAFS study on Sr^{2+} in aqueous solution, D'Angelo et al.[13] also include scattering contributions from hydrogen and report first-shell distances of 2.64 Å for Sr−O and 3.40 Å for Sr−H. This value of the Sr−H distance corresponds to water in the dipole orientation, although this seems unlikely given what is known about the hydration structure around Sr^{2+}. For aqueous Sr^{2+}, the hydration structure is expected to be somewhat more disordered because of the substantially larger ionic radius of Sr^{2+} compared to its alkaline-earth neighbor Ca^{2+}. Thus the thermal "wagging" motions should significantly shorten the mean Sr−H distance. In a more recent study of Ni^{2+} hydration by the same group,[43] the Ni−H distance from EXAFS is again close to the maximum expected in the dipole orientation and about 0.1 Å longer than that derived from neutron scattering.[44] The source of this discrepancy is not known.

Ca^{2+} in Mixed Solution with $MgCl_2$ and in the Hexahydrate Melt. The results of EXAFS analysis for a mixed solution containing 0.7 *m* $CaCl_2$ and 5 *m* $MgCl_2$ are reported as item "E" in Table 1. Because of its much smaller ionic radius, the waters of hydration around Mg^{2+} are more tightly bound than those around Ca^{2+} and there is negligible interaction with Cl^- ions even at high concentration. Thus in the mixed solution, where there is competition for water molecules from large numbers of Mg^{2+} ions, the relatively weakly hydrated Ca^{2+} ion is likely to exhibit increased dehydration and ion-pairing. Although the uncertainties on the coordination numbers are quite large, the EXAFS analysis does indeed indicate a small amount of $Ca^{2+}-Cl^-$ contact ion pair formation. The Ca−O coordination number is also slightly reduced compared to the corresponding result ("C") for 6 *m* $CaCl_2$, which is consistent with the penetration of some Cl^- into the first shell. The fit returns realistic estimates of the Ca−Cl distance and Debye−Waller factor, thus helping to confirm the existence of a small proportion of contact ion pairs.

The EXAFS data collected for the fused ($T = 32$ °C) $CaCl_2 \cdot 6(H_2O)$ standard provides the clearest evidence for the formation of substantial numbers of $Ca^{2+}-Cl^-$ contact ion pairs. The melt serves as a higher-concentration (9.25 *m*) reference for the 6 *m* $CaCl_2$ solution; therefore, the uncorrected, k^2-weighted $\chi(k)$ data have been compared directly in Figure 3. There is a distinct phase shift around $k = 7$ Å^{-1} that can be ascribed to the presence of Cl^- in the inner shell around Ca^{2+}. The absence of a similar change in the comparison already made with a low-concentration reference (again, Figure 3) provides additional confirmation of the lack of significant contact ion-pairing in the concentrated 6 *m* $CaCl_2$ solution. The EXAFS fit to the melt data (item "F" in Table 1) indicates an average of 1.2 Cl^- ions in the first coordination shell around Ca^{2+}, resulting in the displacement of about 1.5 waters. The Ca−O distance is the same as for completely hydrated Ca^{2+} in the aqueous phase and, as expected, the Cl^- resides at a slightly longer distance of 2.75 Å due to the larger hard-sphere radius. The same system has been studied using WAXS by Yamaguchi et al.,[3] who reported first-shell parameters of $N_{Ca-O} = 5.6$ and $R_{Ca-O} = 2.44$ Å for the waters and $N_{Ca-Cl} = 1.0$ and $R_{Ca-Cl} = 2.74$ for Cl^-. As can be seen from Table 1, the findings from the present EXAFS investigation are in excellent agreement with the results of this earlier study.

XANES and Pre-edge Spectra. Figure 8a shows the XANES transmission spectra for the two aqueous Ca^{2+} solutions and the three solid reference compounds. The features at 4039 and 4043.5 eV are assigned to $1s \rightarrow 3d$ and $1s \rightarrow 4p$ transitions, respectively. For the systems that contain only water in the first coordination shell, namely, the 0.2 *m* $Ca(ClO_4)_2$ solution and $CaCl_2 \cdot 6(H_2O)$ solid, a large XANES peak is evident near 4049 eV. This feature is primarily a result of Ca−O single scattering in the first shell, although there are weak secondary contributions from the second hydration shell and from first-shell multiple scattering. In the case of the other two reference systems, solid $CaCl_2$ and $CaCl_2 \cdot (H_2O)$, for which the crystal structures show mainly Cl^- in the first coordination shell, the coupling to the $1s \rightarrow 4p$ transition is much more intense. In addition, the large Ca−O XANES peak at 4049 eV, observed for fully hydrated Ca^{2+}, is now replaced by weaker Ca−Cl scattering peaks. The XANES spectrum for the 6 *m* $CaCl_2$ solution appears to be intermediate between those of the 0.2 *m* $Ca(ClO_4)_2$ solution and the $CaCl_2 \cdot 6(H_2O)$ solid, while lacking any of the distinct characteristics of the systems containing inner-shell Cl^-. Not only is this consistent with fully hydrated Ca^{2+} ions but also it suggests the presence of appreciable numbers of Cl^- ions in the *second* coordination sphere as this is also a feature of the crystal structure of $CaCl_2 \cdot 6(H_2O)$. Changes in the pre-edge peak at 4043.5 eV may then be ascribed to the formation of solvent-shared $Ca^{2+}-OH_2-Cl^-$ ion pairs, which would slightly change the $1s \rightarrow 4p$ coupling. We can estimate that there are approximately 5 Cl^- in the second shell by comparing the height of this feature to that for the $CaCl_2 \cdot 6(H_2O)$ solid where there are 8 second-shell Cl^- and to that for the 0.2 *m* $Ca(ClO_4)_2$ solution where there are none. Support for this result comes from a WAXS study on 6.45 *m* $CaCl_2$ aqueous solution by

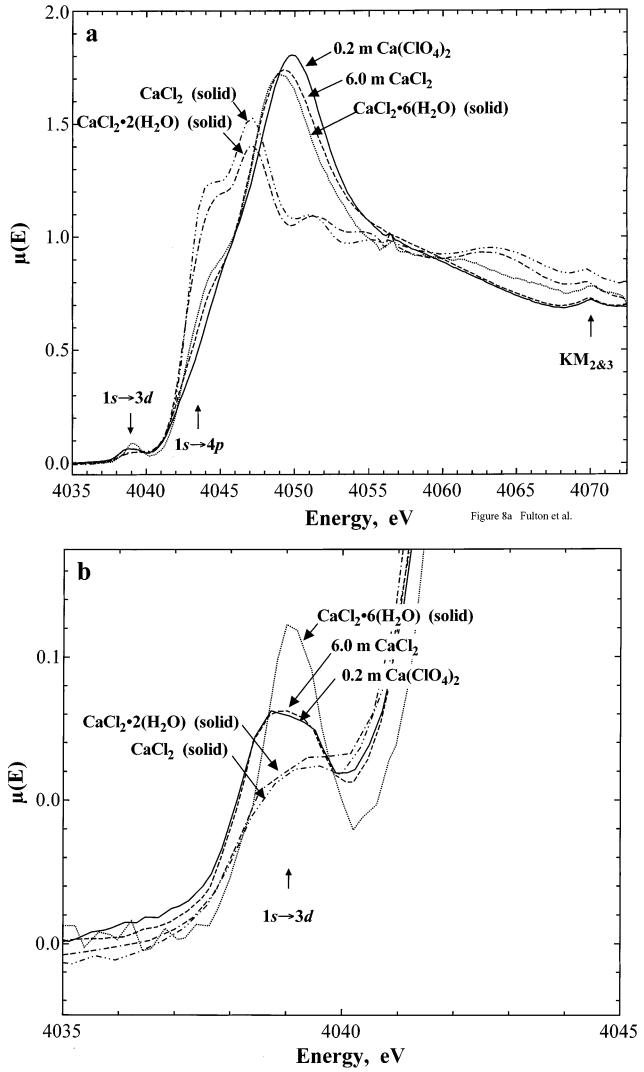

Figure 8. XANES and pre-edge spectra at the Ca K-edge for the three solid standards, and the 0.2 *m* $Ca(ClO_4)_2$ and 6.0 *m* $CaCl_2$ solutions. The vertical arrows in (a) indicate the features corresponding to the 1*s* → 3*d*, 1*s* → 4*p*, and $KL_{II,III}$ transitions. In (b) the edge region is expanded about the 1*s* → 3*d* transition. All spectra are scaled to a common edge-height and were measured in transmission mode.

Yamaguchi et al.,[3] where least-squares modeling of the data indicates approximately 6 Cl^- ions in the second hydration shell around Ca^{2+}. Given the lack of change in the nearest-neighbor environment of Ca^{2+}, the formation of such solvent-shared ion pairs would appear to be the primary structural change in concentrated $CaCl_2$ aqueous solutions—at least in the concentration range up to about 6 *m*.

An expanded view of the 1*s* → 3*d* region is shown in Figure 8b. This transition is formally forbidden for octahedral symmetries. Hence, for the two solid compounds that have an octahedral structure, $CaCl_2$ and $CaCl_2 \cdot 2(H_2O)$, this band is only weakly evident. However, through either quadrupolar coupling or thermal disorder, some *p*-character mixing can occur, which would destroy the inversion symmetry and thus produce a more intense 1*s* → 3*d* transition. Thus, for example, in the case of $CaCl_2 \cdot 6(H_2O)$, where the 9-fold coordination structure is clearly not octahedral, the transition is significantly more pronounced. The 1*s* → 3*d* bands for the two solution spectra are nearly identical, with an intensity intermediate between that for $CaCl_2 \cdot 6(H_2O)$ and the solids with octahedral structures. This suggests the first-shell Ca^{2+} structure in aqueous solution is distorted with respect to a regular octahedral symmetry, which would be consistent with the results of our earlier EXAFS analysis showing a coordination number of 7 (not 6) and the lack of any significant multiple scattering contributions originating from a symmetric octahedral structure. The fact that the 1*s* → 3*d* band appears to be virtually identical for both solutions also suggests that the formation of solvent-shared ion pairs does not have much effect on first-shell symmetry.

Conclusions

The EXAFS results described in this paper present a consistent picture of the first-shell structure around Ca^{2+} in concentrated aqueous solution. The data for a 6 *m* solution of calcium(II) chloride, particularly when compared to a dilute solution of the perchlorate, provides no evidence for the formation of significant numbers of $Ca^{2+}-Cl^-$ contact ion pairs. The mean water coordination number of about 7 and Ca−O nearest-neighbor distance of 2.44 Å are also both consistent with earlier measurements on less concentrated solutions. Comparing the pre-edge and XANES spectra for the solutions to those of reference compounds, such as the crystalline hydrates, confirms the essential picture of fully hydrated Ca^{2+} ions, even up to concentrations as high as 6 *m*. Only when the concentration is increased still further, for example, in the case of the fused hexahydrate (9.25 *m* $CaCl_2$), is there clear evidence for significant numbers of Cl^- ions in the inner shell around Ca^{2+}. Given that the observed thermodynamic anomaly in these solutions first appears at much lower concentration (around 4.5 *m*), it seems unlikely that the formation of substantial numbers of contact ion pairs is responsible for this phenomenon as originally suggested by Phutela and Pitzer.[8] Instead, our results suggest the primary structural change in concentrated $CaCl_2$ aqueous solutions, at least up to about 6 *m* concentration, is overlap of the first hydration shells around each ion, i.e., the formation of solvent-shared ion pairs. In addition, our results confirm the characteristically low symmetry and disordered nature of the first coordination shell around the hydrated Ca^{2+} ion. The relatively weak nature of the Ca^{2+}−water interaction is also confirmed by the behavior in mixed $MgCl_2-CaCl_2$ aqueous solutions, where the $Ca^{2+}-Cl^-$ contact ion-pairing is promoted by a large excess of free Cl^- from the salt of the fully dissociated and more strongly hydrated Mg^{2+} ions. Our EXAFS measurements also reveal a previously unreported multielectron excitation edge at $k = 10.2$ Å^{-1}, which is ascribed to $KL_{II,III}$ transitions. The inclusion of this new transition, along with the other known $KM_{II,III}$ and KM_I transitions, in the background correction procedure leads to significantly improved EXAFS fits. Further improvements result from the inclusion of Ca−H scattering paths and yield a Ca−H distance of 2.97 Å, a value that is in remarkably good agreement with neutron scattering measurements. This appears to be the most convincing evidence to date for the detection of hydrogen backscattering in EXAFS measurements of aqueous solutions. In a follow-up paper (II), we discuss the results of a complementary neutron diffraction experiment on concentrated $CaCl_2$ solutions, making full use of the insights gained from the present EXAFS study.

Acknowledgment. Work by J.L.F. was supported by the Office of Energy Research, Office of Basic Energy Sciences, Chemical Sciences Division of the U.S. Department of Energy, under contract DE-AC06-76RLO 1830 with Pacific Northwest National Laboratory. Work by Y.S.B. and J.M.S. was supported by the Division of Chemical Sciences, Geosciences, and Biosciences, Office of Basic Energy Sciences, U.S. Department of Energy under Contract DE-AC05-00OR22725 with Oak

Ridge National Laboratory, managed and operated by UT-Battelle, LLC. PNC-CAT facilities and research at these facilities is supported by the US DOE Office of Science grant no. DE-FG03-97ER45628. Use of the Advanced Photon Source was supported by the U.S. Department of Energy, Office of Science, Office of Basic Energy Sciences, under Contract No. W-31-109-ENG-38.

Supporting Information Available: More data on the structure of the multielectron edges and an XAFS fitting evaluation of the C_3 parameter is available. This material is available free of charge via the Internet at http://pubs.acs.org.

References and Notes

(1) Jalilehvand, F.; Spångberg, D.; Lindqvist-Reis, P.; Hermansson, K.; Persson, I.; Sandström, M. *J. Am. Chem. Soc.* **2001**, *123*, 431−441.
(2) Spångberg, D.; Hermansson, K.; Lindqvist-Reis, P.; Jalilehvand, F.; Sandström, M.; Persson, I. *J. Phys. Chem. B* **2000**, *104*, 10467−10472.
(3) Yamaguchi, T.; Hayashi, S.; Ohtaki, H. *Inorg. Chem.* **1989**, *28*, 2434−2439.
(4) Licheri, G.; Picacaluga, G.; Pinna, G. *J. Chem. Phys.* **1976**, *64*, 2437.
(5) Hewish, N. A.; Neilson, G. W.; Enderby, J. E. *Nature* **1982**, *297*, 138−139.
(6) Ohtaki, H.; Radnai, T. *Chem. Rev.* **1993**, *93*, 1157−1204.
(7) Gavin D.; Parker, V. B.; White, H. J., Jr. *CODATA Thermodynamic Tables, Selections for Some Compounds of Calcium and Related Mixtures: A Prototype Set of Tables*; Hemisphere Publishing Corp.: Washington, D.C., 1987.
(8) Phutela, R. C.; Pitzer, K. S. *J. Sol. Chem.* **1983**, *12*, 201−207.
(9) McMillan, W. G.; Mayer, J. E. *J. Chem. Phys.* **1945**, *13*, 276.
(10) Hoffmann, M. M.; Darab, J. G.; Palmer, B. J.; Fulton, J. L. *J. Phys. Chem. A* **1999**, *103*, 8471−8482.
(11) Seward, T. M.; Henderson, C. M. B.; Charnock, J. M.; Driesner, T. *Geochim. Cosmochim. Acta* **1999**, *63*, 2409−2418.
(12) Wilson, K. R.; Tobin, J. G.; Ankudinov, A. L.; Rehr, J. J.; Saykally, R. J. *Phys. Rev. Lett.* **2000**, *85*, 4289−4292.
(13) D'Angelo, P. D.; Nolting, H. F.; Pavel, N. V. **1996**, *53*, 798−805.
(14) Badyal, Y. S.; Barnes, A. C.; Simonson, J. M. *J. Phys. Chem. A*, in preparation.
(15) Tan, Z.; Budnick, J. I.; Heald, S. M. *Rev. Sci. Instrum.* **1989**, *60*, 1021−1025.
(16) Heald, S. M. In *X-ray Absorption: Principles, Applications, Techniques of EXAFS, SEXAFS and XANES*; Koningsberger, D. C., Prins, R., Eds.; John Wiley & Son: New York, 1988; pp 87−118.
(17) Teo, B. K. *EXAFS: Basic Principles and Data Analysis*; Springer-Verlag: New York, 1986.
(18) Stern, E. A.; Heald, S. In *Handbook of Synchrotron Radiation*; Eastman, D. E., Farge, Y., Koch, E. E., Eds.; North-Holland: Amsterdam, 1983.
(19) *X-ray Absorption: Principles, Applications, Techniques of EXAFS, SEXAFS and XANES*; Koningsberger, D. C., Prins, R., Eds.; John Wiley & Sons: New York, 1988.
(20) Stern, E. A.; Newville, M.; Ravel, B.; Yacoby, Y.; Haskel, D. *Physica B* **1995**, *208 & 209*, 117−120.
(21) Newville, M.; Livins, P.; Yacoby, Y.; Rehr, J. J.; Stern, E. A. *Phys. Rev. B* **1993**, *47*, 14126−14131.
(22) Zabinsky, S. I.; Rehr, J. J.; Ankudinov, A.; Albers, R. C.; Eller, M. J. *Phys. Rev. B* **1995**, *52*, 2995−3009.
(23) Newville, M.; Ravel, R.; Haskel, D.; Rehr, J. J.; Stern, E. A.; Yacoby, Y. *Physica B* **1995**, *208 & 209*, 154−156.
(24) Busing, W. R. *Trans. Am. Cryst. Assoc.* **1970**, *6*, 57−72.
(25) Leclaire, A.; Borel, M. M. *Acta Crystallogr.* **1977**, *B33*, 1608−1610.
(26) Agron, P. A.; Busing, W. R. *Acta Crystallogr.* **1986**, *C42*, 141−143.
(27) Frenkel, A. I.; Korshin, G. V.; Ankudinov, A. L. *Environ. Sci. Technol.* **2000**, *34*, 2138−2142.
(28) D'Angelo, P.; Di Nola, A.; Filipponi, A.; Pavel, N. V.; Roccatano, D. *J. Chem. Phys.* **1994**, *100*, 985−994.
(29) Wallen, S. L.; Palmer, B. J.; Pfund, D. M.; Fulton, J. L.; Newville, M.; Ma, Y.; Stern, E. A. *J. Phys. Chem. A* **1997**, *101*, 9632−9640.
(30) D'Angelo, P.; Di Cicco, A.; Filipponi, A.; Pavel, N. V. *Phys. Rev. A* **1993**, *47*, 2055−2063.
(31) Zhang, K.; Stern, E. A.; Rehr, J. J.; Ellis, F. *Phys. Rev. B* **1991**, *44*, 2030−2039.
(32) Li, G.; Bridges, F.; Brown, G. S. *Phys. Rev. Lett.* **1992**, *68*, 1609−1612.
(33) Filipponi, A. *Physica B* **1995**, *208 & 209*, 29−32.
(34) Fulton, J. L.; Hoffmann, M. H. In preparation.
(35) Deslattes, R. D.; LaVilla, R. E.; Cowan, P. L.; Henins, A. *Phys. Rev. A* **1983**, *27*, 923−933.
(36) Eisenberger, P.; Brown, G. S. *Solid State Commun.* **1979**, *29*, 481−484.
(37) Wallen, S. L.; Palmer, B. J.; Fulton, J. L. *J. Chem. Phys.* **1998**, *108*, 4039−4046.
(38) Filipponi, A.; D'Angelo, P.; Pavel, N. V.; Di Cicco, A. *Chem. Phys. Lett.* **1994**, *225*, 150−155.
(39) Fulton, J. L.; Hoffmann, M. M.; Darab, J. G.; Palmer, B. J.; Stern, E. A. *J. Phys. Chem. A* **2000**, *104*, 11651−11663.
(40) Szász, Gy. I.; Dietz, W.; Heinzinger, K. *Chem. Phys. Lett.* **1982**, 388−392.
(41) Powell, D. H.; Neilson, G. W. *J. Phys. Condens. Matter* **1990**, *2*, 3871−3878.
(42) Lightstone, F. C.; Schwegler, E.; Hood, R. Q.; Gygi, F.; Galli, G. *Chem. Phys. Lett.* **2001**, *343*, 549−555.
(43) D'Angelo, P.; Barone, V.; Chillemi, G.; Sanna, N.; Meyer-Klaucke, W.; Pavel, N. V. *J. Am. Chem. Soc.* **2002**, *124*, 1958−1967.
(44) Enderby, J. E. *Chem. Soc. Rev.* **1995**, 159−168.